

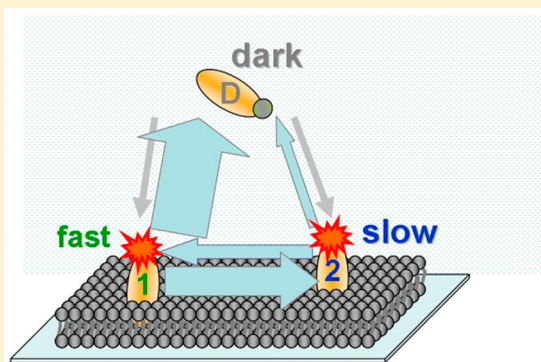
# Single-Particle Tracking Reveals Switching of the HIV Fusion Peptide between Two Diffusive Modes in Membranes

Maria Ott\*,†,§ Yechiel Shai,‡ and Gilad Haran\*,†

†Departments of Chemical Physics and ‡Biological Chemistry, Weizmann Institute of Science, Rehovot 76100, Israel

## Supporting Information

**ABSTRACT:** Fusion of the HIV membrane with that of a target T cell is an essential first step in the viral infection process. Here we describe single-particle tracking (SPT) studies of a 16-amino-acid peptide derived from the HIV fusion protein ( $\text{FP}_{16}$ ), as it interacts with a supported lipid bilayer.  $\text{FP}_{16}$  was found to spontaneously insert into and move within the bilayer with two different modes of diffusion, a fast mode with a diffusion coefficient typical of protein motion in membranes and a much slower one. We observed transitions between the two modes: slow peptides were found to speed up, and fast peptides could slow down. Hidden Markov model analysis was employed as a method for the identification of the two modes in single-molecule trajectories and analysis of their interconversion rates. Surprisingly, the diffusion coefficients of the two modes were found to depend differently on solution viscosity. Thus, whereas the fast diffusive mode behaved as predicted by the Saffman–Delbrück theory, the slow mode behaved according to the Stokes–Einstein relation. To further characterize the two diffusive modes,  $\text{FP}_{16}$  molecules were studied in bilayers cooled through their liquid crystalline-to-gel phase transition. Our analysis suggested that the slow diffusive mode might originate from the formation of large objects, such as lipid domains or local protrusions, which are induced by the peptides and move together with them.



## INTRODUCTION

Infection by HIV is accomplished by successful fusion between its membrane and the T-cell's membrane, as well as by its ability to evade the immune response against it. In order to fuse with the target cell, HIV virions express the envelope glycoprotein gp160, which is composed of gp120–gp41 subunits. The gp120 glycoprotein binds to a cellular receptor (CD4) and a coreceptor (CXCR4 or CCR5).<sup>1</sup> Following the attachment of gp120, gp41 undergoes conformational changes that enable it to catalyze the fusion between the viral and cellular membranes, or between infected and native cells.<sup>2,3</sup> gp41 is composed of several functional regions, of which the fusion peptide ( $\text{FP}_{16}$ ), a 16-amino-acid hydrophobic domain, is responsible for inserting into the host cell membrane and inducing membrane mixing.<sup>4–7</sup> In order to better understand the complex behavior of the fusion peptide and its interaction with cellular receptors, the dynamics of each component need to be better understood. Indeed, multiple studies of the interaction of  $\text{FP}_{16}$  and related molecules with membranes have been performed.

The secondary structures of membrane-inserted  $\text{FP}_{16}$  molecules (or molecules of the slightly longer variant  $\text{FP}_{23}$ ) were found to form either a monomeric  $\alpha$ -helical structure or an oligomeric  $\beta$ -sheet structure.<sup>8–15</sup> The structural plasticity of the peptide allowing it to form the two secondary structures can be related to its fusogenic function.<sup>16–19</sup> However, the  $\alpha$ -helical structure seems to be preferred at low peptide/lipid molar ratios, whereas the  $\beta$ -sheet structure was implicated at higher

peptide/lipid molar ratios.<sup>10</sup> Only at peptide/lipid ratios below 1/2000 all peptides were found to be monomeric.<sup>10</sup> The  $\beta$ -sheet structure found at higher concentrations involves parallel or antiparallel alignment of the strand of a small number of molecules, e.g., trimers.<sup>8,15</sup> Notably, the  $\beta$ -sheet structure cannot be observed by fluorescence techniques, as the proximity dyes in adjacent strands (intermolecular distance is about 2–3 nm) should cause the fluorescence to be efficiently quenched.<sup>20</sup>

Monte Carlo simulations have elucidated the precise intra-membrane arrangement of  $\text{FP}_{23}$ , which contains a short polar sequence in addition to the hydrophobic amino acid stretch of  $\text{FP}_{16}$ . It was found that  $\text{FP}_{23}$  inserts fully into the bilayer and that the  $\alpha$ -helix is oriented at 40° to the surface normal.<sup>21</sup> However, there are also indications that the  $\alpha$ -helix form may in some cases be orientated in parallel to the lipid water surface<sup>13,8,22</sup> and that  $\text{FP}_{16}$  inserts only in the outer leaflet.<sup>22</sup> It is likely that the more hydrophobic nature of  $\text{FP}_{16}$  draws it into the hydrophobic interior of the bilayer.<sup>13</sup>

As a first step toward a quantitative characterization of the dynamics of the HIV fusion peptide on the single molecule level, we used single-particle tracking (SPT) to follow the dynamics of interaction of  $\text{FP}_{16}$  with supported bilayers. This short peptide

**Special Issue:** Peter G. Wolynes Festschrift

**Received:** April 21, 2013

**Revised:** August 3, 2013

**Published:** August 5, 2013

meets nicely the requirements of such an experiment, since it can be dissolved in aqueous buffer solution and inserts spontaneously from the buffer into the membrane.<sup>10,14,15</sup> This allows controlled addition of the peptide during the experiments and prevents the complexity arising from (potential) interactions with the glass support (see discussion in ref 23). Furthermore, at the low concentrations required for these experiments (we used a peptide to lipid ratio <1:10<sup>6</sup>), the peptides insert into the membrane in a monomeric form.<sup>10</sup> By recording the two-dimensional motion of individual particles, SPT can reveal subpopulations, immobile particles, and other heterogeneities which are hidden in the ensemble average by methods like fluorescence correlation spectroscopy<sup>24</sup> and fluorescence recovery after photobleaching.<sup>25</sup> However, the extraction of dynamic information from single-particle trajectories is challenging, since experimental uncertainties are directly coupled to the measurement of the system dynamics.

Several analytical methods have been proposed in order to extract diffusive information from SPT data. Mean-squared displacement (MSD) analysis is the most familiar one.<sup>26</sup> It allows tracking the time development of the average diffusive motion of all particles and enables identifying different types of diffusion: normal or anomalous Brownian motion, confined or corralled motion. Other methods, like jump-distance analysis (JDA)<sup>27</sup> and the related construction of a cumulative probability function (CPF),<sup>28</sup> are based on single-step distributions. They allow extracting subpopulations and revealing their specific diffusion coefficients.

Several difficulties remain in the implementation of the above methods to the analysis of SPT data. First, they fail to consider the influence of noise on the apparent diffusion coefficients. When detection is based on fluorescence, the uncertainty in the determination of the position of a single particle arises from the limited photon number.<sup>29</sup> An increase of the average photon number per unit time (e.g., by increasing the illumination intensity) would in fact reduce the noise. However, as a single fluorophore has only a limited number of photoemission cycles, related to its photochemical lifetime,<sup>30</sup> this improvement is "paid" by a shortening of the available observation time per molecule, which often involves the loss of dynamic information. A second issue related to noise involves sorting out from a data set those particles that are truly immobile. This is particularly difficult when slowly diffusing molecules are involved, and their motion needs to be discriminated from the apparent motion of immobile particles due to the localization error. It should be noted that a slow diffusing fraction has almost always been observed in other experiments on membrane diffusion regardless of the experimental approaches.<sup>25,31–39</sup> However, the origin of the slowly moving fraction is still abstruse and different proposals were put forward, including the involvement of membrane defects,<sup>31</sup> interleaflet coupling,<sup>32</sup> weakly bound vesicles,<sup>33</sup> or transient adsorption of tracer molecules onto the glass support.<sup>34</sup> The slow diffusive mode, often discarded from analysis, might yield important information on the complexity of the interaction of protein molecules with membrane components.

Finally, even more challenging is the identification of discrete dynamic changes within single-molecule trajectories, e.g., transition between slow and fast diffusive modes. The large expected overlap of the jump distance probability distributions and the lack of sufficient averaging calls for the application of reliable statistical approaches that can sort such complex dynamics.

In the present paper, we report SPT data on FP<sub>16</sub> molecules interacting with supported PC bilayers. It was found that the molecules inserted themselves transiently into the membrane, and readily switched between two diffusive modes. We apply a

maximum likelihood method based on hidden Markov models (HMM)<sup>40</sup> to SPT data to identify different diffusive modes of molecules. Alternative maximum likelihood methods were recently discussed, e.g., by Montiel et al.<sup>41</sup> and Elliot et al.<sup>42</sup> HMM analysis is a powerful tool to reveal multistate kinetics in stochastic data, and has been used in varied fields, from speech recognition to single ion channel recording. In the context of SPT, HMM was recently used by Coombs and co-workers for two-state analysis of slowly diffusing LFA-1 molecules on live T-cells<sup>43</sup> as well as by Persson and co-workers to reveal interactions between RNA molecules.<sup>44</sup> Here we show how HMM can be applied for a three-state scenario, in which peptide molecules insert into a supported membrane, diffuse with two possible diffusion coefficients, and then escape back to solution. This scenario is particularly relevant for FP<sub>16</sub>, which, as mentioned above, is soluble in aqueous buffer solution at the concentrations suitable for single-molecule studies, and inserts from the buffer into the membrane, where it is able to switch between two different diffusive modes.

## MATERIALS AND METHODS

**Materials.** The phospholipids egg phosphatidylcholine (EPC), dimyristoyl phosphatidylcholine (DMPC), and lissamine rhodamine phosphatidylethanolamine (1,2-dioleoyl-sn-glycero-3-phosphoethanolamine-N-(lissaminerhodamine B sulfonyl) 18:1) (LissRhod-PE) were purchased from Avanti Polar Lipids Inc. The 16-amino-acid-long FP<sub>16</sub> was synthesized and labeled with 5-carboxytetramethyl-rhodamine, succinimidyl ester as described in ref 45, and kept in a DMSO stock solution at -20 °C. Fluorescent beads (TetraSpeck 0.1 μm, Molecular Probes, USA) were prepared for imaging by first adsorbing them onto a glass slide and then covering them by a mounting gel (Aqua-Poly/Mount, PolySciences, Inc.) and a second glass slide.

**Supported Bilayer Preparation.** An important issue which often hampers direct comparison of experimental results is the protocol of membrane preparation. For the sake of simplicity and comparability, we used a glass support (Paul Marienfeld GmbH) to generate phospholipid bilayers by vesicle fusion. Supported bilayers of EPC were prepared as previously described, using 50 mM Tris buffer at pH 7.5.<sup>46</sup> For experiments with tracer lipid molecules, we added LissRhod-PE dissolved in chloroform prior to the lipid lyophilization step, to reach a final concentration of 2 × 10<sup>-6</sup> mol %. The preparation of DMPC bilayers followed the same protocol, but during vesicle fusion, the sample was heated by a hot water bath at 50 °C ( $T_m + 27$  °C) to allow spreading of the lipids.

**Measurements.** Experiments were performed on a total internal reflection microscope with a temperature controlled sample unit as described in detail in section S1 of the Supporting Information. Experiments with FP<sub>16</sub> molecules labeled at their N terminus with 5-carboxytetramethyl-rhodamine were initiated by exchanging the solution above a supported bilayer with a buffer solution containing the peptide molecules at a concentration of ~10–20 pM. This concentration was selected so that only ~10 fluorescent molecules were found in each camera frame. Higher molecular densities would possibly lead to wrong connections between molecules in consecutive camera frames generated by the tracking procedure (see below). Each measured frame corresponded to a membrane area of 22 × 22 μm<sup>2</sup>. At acquisition frequencies above 100 Hz, a reduction of the exposed detector area was required. For instance, at 150 Hz, the window size was 11 × 22 μm<sup>2</sup>. If it occurred that the fraction of mobile molecules was less than 10% (for example, in experiments close to the transition temperature of DMPC membranes), the

concentration of peptide molecules in the solution was increased, but immobile molecules were photobleached prior to data acquisition, as described in ref 47.

Under each experimental condition, sets of 3000 frames were recorded at least at 10 different positions on the sample, providing about 5000–20 000 traces of single molecules passing the criterion of mobility (see below). This data set size guaranteed representative and reproducible data. It was verified that the results are independent of the time that passed between buffer exchange and data collection.

Control experiments showed that the short-lived fast diffusive mode is not affected by photobleaching, whereas the long-lived slow diffusive mode is slightly affected if the laser power is increased (Figure S2, Supporting Information). Therefore, the laser excitation intensity was selected such that the effect of photobleaching was minimal and could be neglected. We found no further improvement upon adding oxygen scavenger systems, like ascorbic acid.<sup>48</sup> Long-time blinking of the fluorophores, which could in principle hamper the detection of long trajectories, was found to be of minor importance in our experiments, as tested by studying immobile molecules. Indeed, some immobile labeled FP<sub>16</sub> molecules could be easily detected up to 2000 consecutive frames. The effect of the acquisition frequency on the retrieved diffusion coefficients was carefully checked (Figure S3, Supporting Information). On the basis of our findings for fast diffusion coefficients, data acquisition was carried out at frame rates of 50 and 100 Hz for each point in Figure 5 and 30, 100, and 150 Hz for each point in Figure 6. To verify the value of the slow diffusion coefficients, additional 10 Hz data sets were acquired in most cases.

Single-molecule trajectories were calculated from the data using home-written programs that allowed us to detect and localize molecules following the approach of ref 49, to connect the nearest neighbor molecules in consecutive frames as shown in ref 50, and to apply different analysis methods on the detected trajectories. The tracking algorithms are briefly described in the section S4 of the Supporting Information. A minimal trajectory length of three steps was imposed as a condition for the analysis of the particle diffusion. Details of the analysis methods applied to the trajectories can be found as well in the Supporting Information (section S5).

**Selecting Mobile Molecules.** As discussed in the Introduction, the localization noise complicates the discrimination of immobile particles from slowly moving ones. We developed a method that allowed us to reliably identify immobile particles and exclude them from the analysis. The criterion for identifying immobile particles relies on calculating the variance of the displacement of each particle with respect to its mean position,  $\langle(\Delta r_m)^2\rangle$ :

$$\langle(\Delta r_m)^2\rangle = \frac{1}{N_{\text{pos}} - 1} \sum_i^{N_{\text{pos}}} [(x_i - x_m)^2 + (y_i - y_m)^2] \quad (1)$$

with  $(x_i, y_i)$  describing the  $i$ th position of the particle and  $(x_m, y_m)$  the mean of all its  $N_{\text{pos}}$  detected positions. We use  $\langle(\Delta r_m)^2\rangle$  rather than, say, the MSD (eqs S2 and S5, Supporting Information), since for a fixed particle  $\langle(\Delta r_m)^2\rangle$  is equivalent to the error of localization due to photon noise  $\langle(\Delta r_m)^2\rangle = r_{0,\text{noise}}^2$ , while for a moving particle  $\langle(\Delta r_m)^2\rangle > r_{0,\text{noise}}^2$ . To rigorously characterize the error of localization, we resorted to studies of “trajectories” of glass adsorbed fluorescent spheres covered by a fixation gel. Due to the error of localization, a jump distance distribution calculated from the data looks comparable to that of a slowly diffusing particle (Figure S6A, Supporting Information), and a fit to eq 8 would give an apparent  $r_0$  of 70 nm,

which would correspond to a diffusion coefficient of  $0.12 \mu\text{m}^2/\text{s}$  at a frame rate of 100 Hz. However, calculation of the MSD according to eq S5 (Supporting Information) shows complete independence on time, which further proves that the particles do not diffuse (Figure S6B, Supporting Information).

We determined  $r_{0,\text{noise}}$  of the fluorescent spheres as a function of the mean photon number,  $N_{\text{ph}}$ , and also of the length of each trajectory,  $N_{\text{steps}}$ , to account for broadening of the distribution when short trajectories are used.<sup>51</sup> We then defined a threshold value,  $r_{0,\text{noise}}^{\text{th}}$ , beyond which a particle is considered to be mobile, by taking a confidence interval of two standard deviations of the distribution:

$$r_{0,\text{noise}}^{\text{th}}(N_{\text{ph}}, N_{\text{steps}}) = r_{0,\text{noise}}^{\text{mean}}(N_{\text{ph}}) + 2r_{0,\text{noise}}^{\text{dev}}(N_{\text{ph}}, N_{\text{steps}}) \quad (2)$$

In order to determine this threshold, we changed the power of excitation to obtain “trajectories” with a minimum of 10 and a maximum of 10 000 photons per particle. The resulting trajectories were cut into short sequences of different lengths to determine the dependence on  $N_{\text{steps}}$ . Figure S6C (Supporting Information) shows the  $r_{0,\text{noise}}$  distribution of trajectories containing 10 steps as a function of the photon numbers. While the mean value of  $r_{0,\text{noise}}$  is independent of trajectory length and depends only on the photon number (black line), the width of the distribution increases as the trajectories are shortened. We found that  $r_{0,\text{noise}}^{\text{th}}$  follows the following empirical relation:

$$r_{0,\text{noise}}^{\text{th}} = A(N_{\text{steps}})(N_{\text{ph}})^{\beta} \quad (3)$$

with the experimentally derived parameter  $A(N_{\text{steps}}) = [(8.9 \pm 0.3) + (2.0 \pm 0.6) \exp(-(0.06 \pm 0.02)N_{\text{steps}})] \times 10^{-7} \text{ m}$  as plotted in Figure S6D (Supporting Information). The exponent  $\beta$  was determined to be  $-0.52 \pm 0.01$  which is close to the theoretical value of  $-1/2$ .<sup>29</sup>

This threshold criterion enabled us to reliably identify 98.5% of the trajectories of the fixed latex spheres as belonging to immobile particles, independently of their photon number and individual length. This value is in agreement with the expected value of 98.0% for a Gaussian distribution.

## RESULTS AND DISCUSSION

We recorded single-molecule trajectories of FP<sub>16</sub> molecules interacting with supported lipid bilayers. These bilayers were made of EPC, unless otherwise noted. An initial survey of the recorded trajectories showed a large diversity of the diffusive behavior of the monitored molecules (Figure 1). Using the analysis discussed below, we found that 40% of all observed molecules studied at room temperature could be classified as (apparently) immobile (trace i). The other 60% of the molecules were unequivocally classified as freely moving (traces ii–vi). Interestingly, trajectories of mobile FP<sub>16</sub> molecules revealed two modes of diffusion, which we designated “slow” and “fast”. The trajectories of the type presented in Figure 1 demonstrate that transitions between the two diffusive modes could be found in both directions: from the slow to the fast mode (trace iii) as well as from the fast to the slow mode (trace iv). Some traces also showed multiple transitions, like traces v and vi. It should be noted that this behavior could be clearly distinguished from that of unimodal diffusing particles, as discussed below.

The observation of bidirectional switching of the diffusion of FP<sub>16</sub> molecules after they inserted into the membrane and their eventual escape back into solution led us to build a three-state model to describe the dynamics. The three-state Markov model involves transitions from the dark state (D) into one of the

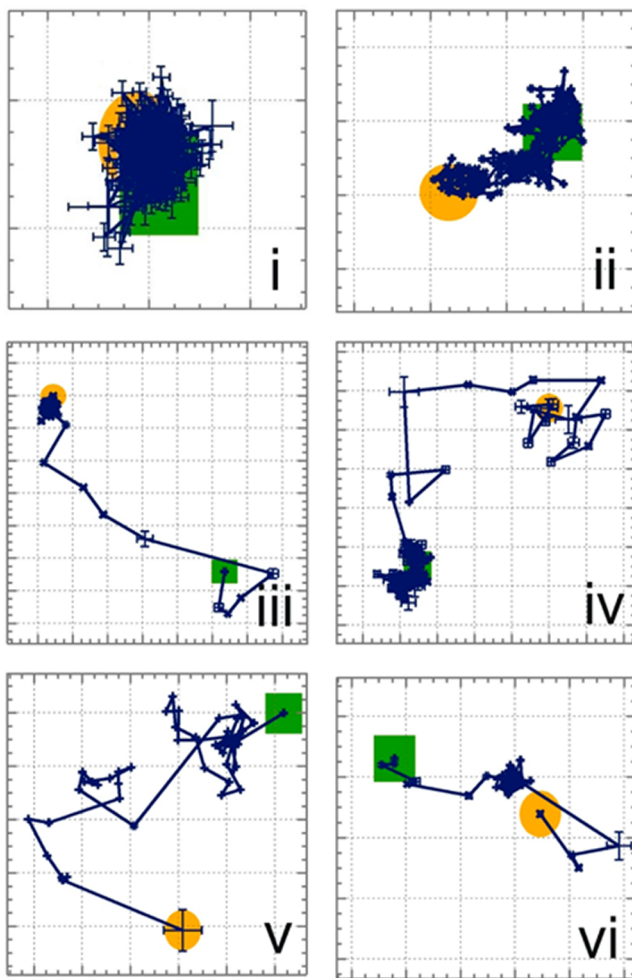


**Figure 1.** Trajectories of  $\text{FP}_{16}$  within the EPC bilayer. The first and last detected positions are marked with an orange circle and a green square, respectively. Each square of the grid depicts one pixel with a size of  $0.177 \times 0.177 \mu\text{m}^2$ .

diffusive fluorescent states (either  $F_1$  or  $F_2$ ). This transition occurs with rates  $k_{D1}$  or  $k_{D2}$ , respectively. Once inserted in the membrane, the molecule is able to switch between the two diffusive modes corresponding to the fast and slow diffusion, respectively, with rates  $k_{12}$  and  $k_{21}$ :



An inverse transition occurs when a peptide leaves the membrane back into solution. The dark state involves peptide molecules in solution (outside the membrane). Since the diffusion in the buffer solution is about three orders of magnitude faster than membrane diffusion, these molecules cannot be detected.

We developed an HMM-based approach complemented with other analytic methods in order to analyze the measurements based on the above kinetic scheme and extract the kinetic constants. Below, we introduce our approach and show how we incorporate knowledge about localization noise into the analysis.

**Analysis of Transitions between Diffusive Modes. A Hidden Markov Model for Three-State Dynamics with Diffusion.** A Markov-chain description of the three-state dynamics introduced in eq 4 can be written as follows:

$$S_j(t + \Delta t) = a_{ij} S_i(t) \quad (5)$$

where  $S_i(t)$  is the probability that the system is in state  $i$  at time  $t$  and the state transition coefficient  $a_{ij}$  is the probability that the system in state  $i$  will undergo a transition to state  $j$  during the time interval  $\Delta t$ . For an infinitely small  $\Delta t$ , the transition probability matrix  $A = \{a_{ij}\}$  of the three-state model can be written as

$$A = \begin{pmatrix} 1 - \Delta t(k_{12} + k_{ID}) & \Delta t k_{12} & \Delta t k_{1D} \\ \Delta t k_{21} & 1 - \Delta t(k_{21} + k_{2D}) & \Delta t k_{2D} \\ \Delta t k_{D1} & \Delta t k_{D2} & 1 - \Delta t(k_{D1} + k_{D2}) \end{pmatrix} \quad (6)$$

The matrix  $A$  is one element of the HMM to be applied to the diffusion data. A second element is the vector of initial state probabilities,  $S_i(0)$ , which in our model reflects the equilibrium relative population of the two diffusive states. Finally, an important characteristic of an HMM is that the states are “hidden”, since they are only observed through a set of experimental observations. The latter are connected to the system states through certain probability density functions. Thus, for single-particle diffusion, the observable is the jump distance of the particle between two consecutive camera frames,  $r$ . The two-dimensional mean-squared distance,  $r_0^2 = \langle r^2 \rangle$ , is related to the diffusion coefficient  $D$  and the time interval  $\Delta t$  between frames:

$$r_0^2 = 4D\Delta t \quad (7)$$

The jump distance distribution is then<sup>28</sup>

$$p(r) = 2 \frac{r}{r_0^2} \exp\left\{-\frac{r^2}{r_0^2}\right\} \quad (8)$$

It is important to note that the localization of single molecules always involves an uncertainty due to the limited number of detected photons. This limitation becomes especially apparent when the diffusion is slow enough so that single steps fall in the range of the uncertainty of localization. In such a case, ignoring the localization noise might lead to false assignment of immobile particles as moving ones, and to the overestimation of the true diffusion coefficient. The apparent jump distance distribution,  $p(r_{\text{app}})$ , can be written as a convolution relation of the jump distance distribution  $p(r)$  and the noise distribution  $n(r)$  (note that the latter affects the measurement both at the beginning and at the end of each single step):

$$p(r_{\text{app}}) = \int p(r)n(r_{\text{app}} - r) dr \quad (9)$$

Hence, for a normally distributed, random noise, we can replace eq 8 by

$$p(r_{\text{app}}) = 2 \frac{r_{\text{app}}}{(r_0^2 + 2r_{0,\text{noise}}^2)} \exp\left\{-\frac{r_{\text{app}}^2}{(r_0^2 + 2r_{0,\text{noise}}^2)}\right\} \quad (10)$$

where  $r_{0,\text{noise}}^2$  is the mean squared displacement due to noise and can be characterized independently in control experiments (see Materials and Methods).  $r_{0,\text{noise}}^2$ , being the noise on the jump size of a two-dimensional diffusion process, is twice the localization noise in each direction,  $r_{0,\text{noise}}^2 = 2\sigma_{\text{noise}}^2$ .  $\sigma_{0,\text{noise}}^2$  depends on the width of the Gaussian function fitted to the fluorescent spot of the molecules,  $s$ , on the number of photons emitted by each molecule,  $N$ , the resolution, given by the camera pixel size,  $a$ , and the background noise of the camera,  $b$ :<sup>29</sup>

$$\sigma_{\text{noise}}^2 = \frac{s^2 + a^2/12}{N} + \frac{8\pi s^2 b^2}{a^2 N^2} \quad (11)$$

Table 1. Analysis of Simulated Trajectories<sup>a</sup>

noise	simulation parameters	no noise <sup>b</sup>	$r_{0,\text{noise}} = 10 \text{ nm}^b$	$r_{0,\text{noise}} = 100 \text{ nm}^b$	$r_{0,\text{noise}} = 100 \text{ nm}^c$
$k_{12}$	4.0	$4.2 \pm 0.3$	$3.9 \pm 0.4$	$4.2 \pm 0.4$	$3.8 \pm 0.4$
$k_{21}$	10.0	$9.7 \pm 0.3$	$9.9 \pm 0.4$	$9.7 \pm 0.2$	$11.0 \pm 0.4$
$k_{1D}$	14.0	$14.3 \pm 0.4$	$14.1 \pm 0.3$	$13.2 \pm 0.2$	$13.3 \pm 0.4$
$k_{2D}$	2.0	$2.0 \pm 0.2$	$2.1 \pm 0.2$	$2.3 \pm 0.4$	$0.6 \pm 0.1$

<sup>a</sup>Rates of interconversion in  $\text{s}^{-1}$  in simulated trajectories with  $D_{\text{fast}} = 1.00 \mu\text{m}^2/\text{s}$  and  $D_{\text{slow}} = 0.05 \mu\text{m}^2/\text{s}$  (corresponding to  $r_{0,1} = 200 \text{ nm}$  and  $r_{0,2} = 45 \text{ nm}$ , respectively), generated at different noise levels  $r_{0,\text{noise}}$ . The error bars show the standard deviation of five independent data sets of 1000 trajectories each. <sup>b</sup>Based on analysis of all simulated traces. <sup>c</sup>Based on analysis of traces that passed the mobility criterion of eq 2 only (83% of all traces).

As noted, the actual implementation of the HMM to the experimental data involved two diffusive states and one dark state. At the end of each trajectory, a marker was set that

denoted the transition to the dark state encoded by a negative value. The probability density function,  $p_i(r)$ , with  $i = 1–3$ , was written as follows:

$$p_i(r) = \begin{cases} \frac{r}{4D_i\Delta t + 2r_{0,\text{noise}}^2(N_{\text{ph}}^i)} \exp\left\{-\frac{r^2}{4D_i\Delta t + 2r_{0,\text{noise}}^2(N_{\text{ph}}^i)}\right\} & \text{for } r \geq 0, i = 1, 2 \text{ (fluorescent)} \\ 1 & \text{for } r < 0, i = 3 \text{ (dark)} \end{cases} \quad (12)$$

The noise parameter was written here as an explicit function of the average number of photons in each state ( $N_{\text{ph}}^i$ ).

The jump distance probability of each state depends on a single unknown parameter, the diffusion coefficient. Additional unknown parameters are the initial state probabilities and the transition probabilities. The HMM analysis provides a route for obtaining these parameters by iteratively maximizing the likelihood of the given sequence of observations obtained in the experiments. On the basis of the Baum–Welch algorithm, re-estimation formulas can be derived for the parameters that take into account the whole data set.<sup>40</sup> For example, the re-estimation formula for the diffusion coefficients is

$$D_i = \frac{1}{4\Delta t} \left( \frac{\sum_j \gamma_{ij} [r_j^2 - 2r_{0,\text{noise}}^2(N_{\text{ph}}^j)]}{\sum_j \gamma_{ij}} \right) \quad i = 1, 2 \quad 1 \leq j \leq N_{\text{step}} \quad (13)$$

where  $\gamma_{ij}$  is the probability of being in state  $i$  at the  $j$ th time step, based on the experimental data and set of parameters determined in the previous iteration. The  $\gamma_{ij}$ 's are calculated by the forward–backward procedure described by Rabiner,<sup>40</sup> who also gives formulas for re-estimation of the transition probabilities and the equilibrium populations. A new parameter set is obtained in each iteration of the Baum–Welch algorithm, and it is mathematically guaranteed that the likelihood is eventually locally maximized.

**Analysis of Simulated Single Molecule Tracks.** To test the analytic scheme outlined above, we simulated sets of trajectories using the three-state rate kinetic model of eq 4, and then applied the HMM methodology to them. Each simulated trajectory started directly after the “insertion” of a peptide molecule. The initial state of the molecule was randomly determined by the stationary probability of the two fluorescent states, and the subsequent states were generated according to the transition probabilities  $a_{ij}$  of eq 6, which also included the probability to leave the system back in the dark state. A termination sequence was appended when the dark state was reached. The state sequence was encoded by jump distances randomly selected according to the characteristic diffusion coefficients of the states using the corresponding probability distributions of eq 8.

Finally, Gaussian noise of a variable amplitude was added to each set of coordinates to test its influence on the data analysis. (For detailed information of the algorithm, see section S7 in the Supporting Information.)

In the analysis of the simulated trajectories, we used the open source HMM toolbox for Matlab.<sup>52</sup> For each data set, we verified that varying the initial set of parameters did not affect the resulting parameters, thus confirming that a global maximum was found and the identification and separation of the two diffusive modes was reliably accomplished. Once a set of parameters that maximized the likelihood was found, we used the Viterbi algorithm to annotate the trajectories and assign data segments to one of the two diffusive states. We applied either JDA or MSD analysis on the set of steps assigned to each of the states for further analysis of the diffusion coefficient. Detailed descriptions of the relevant procedures can be found in the Supporting Information, section S5.

We first analyzed a set of trajectories simulated on the basis of a single diffusive state. Due to the random nature of Brownian motion, even trajectories of particles with a single diffusion coefficient show domains of apparent slower motions,<sup>26</sup> as highlighted in the example of Figure S8A and B (Supporting Information). We applied the three-state HMM analysis to the simulated data set, and found that it reliably identified the set as originating from a unimodal jump size distribution, with less than 1% of the steps assigned to an apparent “slow population” (Figure S8C, Supporting Information). This was even true when the simulation included noise levels of the same range of the mean squared distance ( $r_{0,\text{noise}}^2 \approx r_0^2$ ).

In the case of two-state diffusion simulations, we found the HMM analysis as reliable, and even at high noise levels, the two rates of interconversion were found to be very well determined (Table 1). Figure 2A shows examples of simulated trajectories (100 Hz acquisition rate) with switches between two diffusion coefficients,  $D_1 = 1 \times 10^{-12} \mu\text{m}^2/\text{s}$  ( $r_{0,1} = 200 \text{ nm}$ ) and  $D_2 = 0.05 \times 10^{-12} \mu\text{m}^2/\text{s}$  ( $r_{0,2} \approx 45 \text{ nm}$ ), and at a noise level of  $r_{0,\text{noise}} = 10 \text{ nm}$ . As the figure shows, the HMM analysis allowed us not only to determine the characteristic diffusion coefficients of the diffusive states but also to assign each step in a trajectory to one of the states, using the Viterbi algorithm, which opened the way to

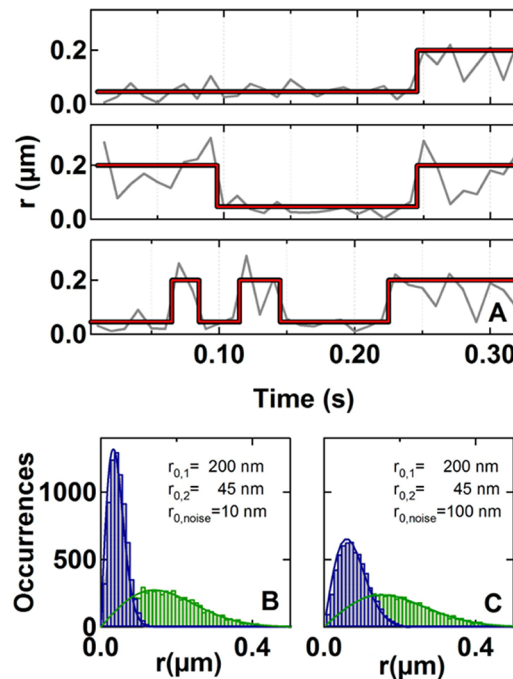


**Figure 2.** Analysis of simulated trajectories: (A) Sample simulated single-molecule trajectories of diffusing particles with slow and fast modes (gray) after addition of noise ( $r_{0,\text{noise}} = 10 \text{ nm}$ ) together with the true (black) and HMM estimated (red) state annotation. (B, C) Jump size distributions were calculated from sequences of single-molecule trajectories identified in the HMM analysis as belonging to the slow or fast mode (blue or green, respectively). (C) Same as in part B but from simulations with  $r_{0,\text{noise}} = 100 \text{ nm}$ .

additional characterizations of the diffusive states. The Viterbi analysis of the whole set of simulated trajectories showed that 95% of all single steps were correctly assigned to the fast or slow state despite the added noise. For comparison, in the absence of localization noise, the level of correct state assignment was about 97%. At the highest noise level, which is twice the mean jump distance in the slow diffusive mode ( $r_{0,\text{noise}} = 100 \text{ nm}$ ), still 92% of the steps were correctly assigned.

The jump size histograms of the individual steps assigned to either of the diffusive states calculated from simulations with noise levels of 10 and 100 nm are shown in Figure 2B and C, respectively. The two selected noise levels roughly correspond to trajectories with quantum yields of 1000 and 100 photons/molecule, respectively. The noise-induced broadening of the jump size distribution at the higher noise level is evident in panel C. The HMM analysis correctly picks up the dynamic parameters even in the face of this broadening.

**Analysis of  $\text{FP}_{16}$  Trajectories.** To study the behavior of  $\text{FP}_{16}$ , we collected approximately 30 000 single-molecule trajectories in EPC membranes at room temperature ( $20^\circ\text{C}$ ), as described in the Materials and Methods section. Here we apply the analytical approach introduced above, based on the HMM, to the experimental trajectories and discuss in depth the possible origin of the slow diffusive mode, based on a series of experimental investigations. The analysis was conducted only on molecules that passed the criterion for mobility (about 19 000 traces).

**Three-State Kinetics.** To be able to follow molecules in the fast diffusive mode, typically characterized by a short dwell time, an acquisition frequency of 100 Hz was needed. Frequencies below 50 Hz would have led to a reduced detection of the

short-lived fast diffusive state (see the Supporting Information, section S3). On the other hand, the dwell times of molecules in the slow diffusive state were roughly three times longer and hence required low laser power to avoid fast photobleaching of the fluorescent markers (Supporting Information, section S2).

These experimental restrictions led to a situation in which the noise of localization was above the average jump distance of the slow diffusive mode ( $r_{0,\text{noise}} > r_{0,\text{slow}}$ ). In such a situation, the described threshold criterion assigns to the mobile fraction those particles that either visited the fast diffusive state or, if they were in the slow state only, stayed long enough within the membrane to sufficiently average the noise contribution. Simulations show that this (unavoidable) bias leads to an underestimation of the rate from the slow diffusive state to the dark state but does not affect the other rates. (See the last column of Table 1, where this phenomenon is observed in the analysis of simulated data.)

Application of the three-state HMM analysis to the trajectories resulted in rates as given in Figure 3A. Figure 3B shows the

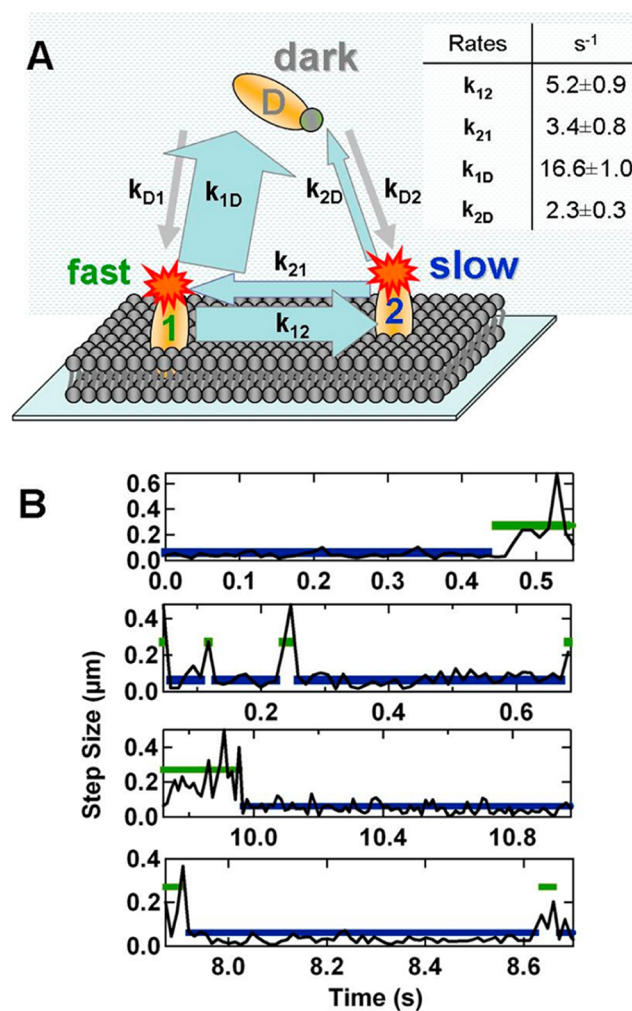


**Figure 3.** HMM analysis of  $\text{FP}_{16}$  molecules interacting with a supported bilayer. (A) Rates obtained from analysis of trajectories measured in an EPC bilayer at  $20^\circ\text{C}$ . (B) Single-molecule trajectories together with HMM mode annotations: the mean distances are shown as green lines for the fast and as blue lines for the slow diffusive mode, respectively. The corresponding 2D trajectories are shown in Figure 1.

trajectories of Figure 1 with state annotations based on the analysis. Dwell time histograms of the two diffusive states

revealed an overall single exponential behavior, which we used as an indication that two states are sufficient to characterize the observed dynamics. It is important to note here that a similar study of the diffusion of fluorescent lipid molecules revealed a single diffusive mode only, although a fraction of 5% immobile molecules was detected here too (Supporting Information, section S9).

The analysis showed that the molecules have a strong tendency to escape back to solution soon after insertion. The leaving rates from the fast and slow states,  $k_{1D}$  and  $k_{2D}$ , were  $16.6 \pm 1.0$  and  $2.3 \pm 0.3 \text{ s}^{-1}$ , respectively.  $k_{2D}$  is biased due to the preferred selection of trajectories that are either long or contain a fast diffusive state, as already discussed. The *true* leaving rate can be estimated to be about  $4 \text{ s}^{-1}$ , a value which is still 4 times smaller than the leaving rate of the fast diffusive state. The rate for the transition from the fast to the slow mode,  $k_{12} = 5.2 \pm 0.9 \text{ s}^{-1}$ , is almost twice as high as its inverse rate,  $k_{21} = 3.4 \pm 0.8 \text{ s}^{-1}$ , which leads together with the fast leaving rate to a lifetime of the fast state that is as short as  $46 \pm 1 \text{ ms}$ .

The rates of insertion,  $k_{D1}$  and  $k_{D2}$ , cannot be obtained from the HMM analysis, as the peptides are not visible while moving in solution. These rates can be estimated from the number of particles appearing on the membrane plane per time interval. For a peptide concentration of  $15 \pm 3 \text{ pM}$ , the rates of insertion into the fast and slow modes were found to be  $0.025 \pm 0.001$  and  $0.005 \pm 0.001 \text{ particles}/(\text{sec}\cdot\mu\text{m}^2)$ , respectively.

**Diffusion Coefficients.** The HMM analysis directly provides the diffusion coefficients of the two modes, which are given in Table 2. However, the ability to assign each step in a trajectory to

**Table 2. Diffusion Coefficients of FP<sub>16</sub> Molecules at 20°C in EPC Bilayers, as Determined by Different Analysis Methods<sup>a</sup>**

analysis method	$D (\mu\text{m}^2/\text{s})$	
	fast	slow
HMM without noise <sup>b</sup>	$2.00 \pm 0.04$	$0.098 \pm 0.055$
HMM with noise correction <sup>c</sup>	$1.85 \pm 0.03$	$0.008 \pm 0.004$
JDA without noise <sup>d</sup>	$1.12 \pm 0.06$	$0.094 \pm 0.047$
JDA with noise correction <sup>e</sup>	$1.05 \pm 0.04$	$0.012 \pm 0.007$
JDA after deconvolution <sup>f</sup>		$0.009 \pm 0.002$
MSD	$1.90 \pm 0.03$	$0.007 \pm 0.001$

<sup>a</sup>The errors are standard deviations based on analysis of four independent data sets. <sup>b</sup>The localization noise was set to 0 in eqs 12 and 13. <sup>c</sup>The localization noise was taken to be  $r_{0,\text{noise}} \approx 22 \text{ nm}$  in eqs 12 and 13. <sup>d</sup>The localization noise was set to 0 in eq 10. <sup>e</sup>The localization noise was taken to be  $r_{0,\text{noise}} \approx 22 \text{ nm}$  in eq 10. <sup>f</sup>According to eq S5.

one of the modes, using the Viterbi algorithm, opened the way to the application of additional analysis methods for validation of the values obtained from the HMM. Figure 4A shows the individual jump distance histograms of the two modes of FP<sub>16</sub>, based on the HMM analysis. We compare below the diffusion coefficients obtained directly from the HMM analysis to two other methods, JDA (Figure 4A) and MSD analysis (Figure 4B), the implementation of which is discussed in detail in section S5 of the Supporting Information.

It appears that the jump distance distribution of the slow state is dominated by the error of localization; hence, analysis without the noise correction included in eqs 8 and 10 would overestimate the diffusion coefficient value by a factor of  $\sim 10$  (see Table 2 and Figure S10A, Supporting Information). However, including the

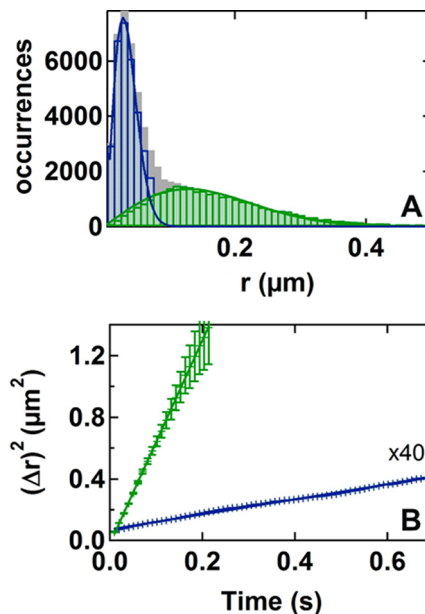


**Figure 4.** Analysis of the two diffusive modes based on the HMM results. (A) Jump size distributions of the fast and slow mode, in green and blue, respectively. (B) Mean square displacements calculated from the data for the two modes. Colors as in part A.

noise leads to agreement between values obtained by analysis using either HMM, JDA, or MSD, with diffusion coefficients of  $(8 \pm 4) \times 10^{-3}$ ,  $(12 \pm 7) \times 10^{-3}$ , and  $(7 \pm 1) \times 10^{-3} \mu\text{m}^2/\text{s}$ , respectively. (The average noise level in the experiment,  $r_{0,\text{noise}}$ , was  $\sim 22 \text{ nm}$ .) We also obtained the diffusion coefficient of the slow mode by deconvolution of the corresponding jump distance distribution with the noise distribution according to eq 9. This approach is advantageous if the noise distribution would appear to be non-Gaussian (which is not the case in our experiments). The deconvolution gives a value of  $(9 \pm 2) \times 10^{-3} \mu\text{m}^2/\text{s}$  and agrees as well with the MSD and HMM results.

The fast diffusion coefficient was less affected by the noise. Nevertheless, the derived diffusion coefficients (after the noise correction) were still found to somewhat depend on the method used for their determination. The coefficients obtained from HMM ( $D = (1.85 \pm 0.03) \mu\text{m}^2/\text{s}$ ) and MSD ( $D = (1.90 \pm 0.03) \mu\text{m}^2/\text{s}$ ) analyses are larger than the coefficient obtained from JDA ( $D = (1.05 \pm 0.04) \mu\text{m}^2/\text{s}$ ). In contrast, the results of the analysis of simulated trajectories generated on the basis of a single diffusive mode did not depend on the method used. This suggests that the jump distance distribution of the fast segments deviates from that of a single diffusive mode. Indeed, a careful analysis of the fast mode distribution revealed a small fraction (5–10%) of long steps, which broadens the distribution beyond the ideal one (see Figure S10B, Supporting Information). This fraction was found to be slightly dependent on laser power, but the origin of these steps is not yet clear. One possibility is that there is a small group of uninserted peptides that are just touching the membrane or sliding at the membrane–buffer interface before vanishing back into solution. Whatever the source of the long steps may be, the JDA is less sensitive to such outliers. Hence, this method gave a more robust estimate for the average diffusion coefficient of the fast mode than MSD or HMM analyses.

To validate the consistency of the above results, we additionally performed CPF analysis, which enables extracting

the diffusion coefficients of the two states as well as the relative fraction of each without the need for the HMM analysis. (The price is of course that no information on the transition kinetics between states is obtained.) A double-exponential fit to the CPF with noise correction (see eq S1, Supporting Information) revealed that about 45% of the mobile FP<sub>16</sub> molecules move with a diffusion coefficient of  $1.45 \pm 0.13 \mu\text{m}^2/\text{s}$ , whereas 55% diffuse apparently much more slowly ( $D = (9 \pm 2) \times 10^{-3} \mu\text{m}^2/\text{s}$ ). The deviation of the value for the fast diffusion from  $1.05 \mu\text{m}^2/\text{s}$  reflects the limitation of a two-component fit, which is evident already if one of the distributions slightly deviates from a Gaussian distribution.

In summary, the HMM analysis allowed us to reliably identify two modes of Brownian motion for FP<sub>16</sub> interacting with glass-supported EPC bilayers, slow and fast. The fast diffusive mode, with a diffusion coefficient of about  $1.05 \mu\text{m}^2/\text{s}$  at  $20^\circ\text{C}$ , corresponds to the diffusive behavior described for other peptides and proteins of similar size in solid-supported bilayers.<sup>53,54</sup> Further, the diffusion is Brownian, as the MSD development is linear with time (Figure 4B). In the slow diffusive mode, the diffusion coefficient is as small as  $8 \times 10^{-3} \mu\text{m}^2/\text{s}$ . However, this diffusive mode was also found to be of Brownian nature and, as time lapse experiments showed, no tendency for confined motion was observed up to a distance of  $1 \mu\text{m}$ .

#### Viscosity and Temperature Effects on FP<sub>16</sub> Dynamics.

To learn more about the dynamics of interaction of FP<sub>16</sub> molecules with supported bilayers, particularly the source of the slow diffusive mode, we performed a series of experiments in which we varied either the viscosity of the buffer covering the supported bilayer or the temperature. As a prelude to the analysis of these experiments, it is worthwhile to briefly discuss the theory of diffusion in membranes and remind the reader of the so-called “continuum fluid hydrodynamic model”, proposed by Saffman and Delbrück.<sup>55</sup> In this theory, which describes the diffusion of cylindrical particles in thin viscous fluid sheets such as free-standing membranes, the diffusion coefficient  $D$  at temperature  $T$  is given by

$$D = \frac{k_B T}{4\pi\eta_m^{**}} [\ln(2L_{SD}/R) - 0.577] \quad (14)$$

In this equation, the Saffman–Delbrück (SD) length,  $L_{SD} = \eta_m^{**}/2\eta_f$  depends on the viscosity of the surrounding solution,  $\eta_f$  and the 2D membrane viscosity,  $\eta_m^{**} = \eta_m h$ , where  $h$  is the thickness of the membrane. The radius of the diffusing particle is given by  $R$ , and  $k_B$  is Boltzmann’s constant. The SD relation is expected to hold when  $R < L_{SD}$ , namely, for small molecules and/or large membrane viscosity.<sup>54,56</sup> An important feature of the SD expression is that the diffusion coefficient has an essentially inverse dependence on the membrane viscosity but depends only logarithmically on the viscosity of the solution.

Equation 14 needs to be corrected for the case of a supported bilayer, where on one side of the membrane there is a nearby solid support.<sup>57,58</sup> In this case, the SD length is replaced by  $b = (2L_{SD})^{1/2}$ , where  $d$  is the distance from the supported bilayer to the solid support and  $L'_{SD} = \eta_m^{**}/(\eta_f + \eta_b)$ , with  $\eta_b$  being the viscosity of the solution between the membrane and the support. Equation 14 now holds in the limit that  $R < b$ , while in the opposite limit,  $R > b$ , a completely different equation is obtained:

$$D = \frac{2k_B T d}{\pi(\eta_f + \eta_b) R^2} \quad (15)$$

In this regime, the diffusion coefficient depends inversely on the solution viscosity, and does not depend on the membrane viscosity. This viscosity dependence is in fact similar to that of a freely diffusing particle, given by the Stokes–Einstein relation. Below, we will compare between results of experiments in which the slow and fast diffusive modes of FP<sub>16</sub> were modulated and these predictions.

**Effect of Solution Viscosity.** We systematically varied solution viscosity by adding increasing concentrations of sucrose to the buffer solution. Sucrose was used in the past to successfully validate the viscosity dependence of the SD equation.<sup>59</sup> We selected sucrose as an additive to the buffer, since we found that the membrane properties of the EPC bilayer were not altered in its presence. When glycerol was used instead, a fraction of more slowly diffusing lipid molecules appeared and the number of immobile FP<sub>16</sub> increased, suggesting specific interactions of the viscofusogen with the membrane. In contrast, the jump size distributions of the lipid tracer LissRhod-PE provided evidence for a single diffusive mode even at high sucrose concentrations, and the reduction of the diffusion coefficient (e.g., by  $(27 \pm 8)\%$ ) at a viscosity of  $9.7 \text{ cP}$  agreed with the prediction from SD theory for a particle of  $0.4 \text{ nm}$  diameter embedded into a membrane with a viscosity of  $1.5 \text{ P}$ <sup>60</sup> and thickness of  $4 \text{ nm}$  (Figure 5).

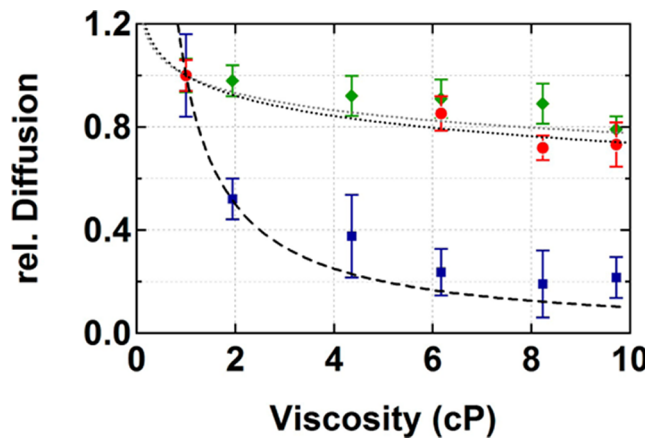


**Figure 5.** Solution viscosity dependence of the diffusion coefficients. Relative diffusion coefficients of the fast (green diamonds) and slow (blue squares) modes of FP<sub>16</sub> and of LissRhod-PE (red circles) as a function of the viscosity of the solution covering the sample. The experimental results are compared with the prediction of SD theory for FP<sub>16</sub> with  $R = 0.9 \text{ nm}$  (black dotted line) and PE with  $R = 0.4 \text{ nm}$  (gray dotted line) and the Stokes–Einstein equation with  $D \sim 1/\eta_f$  (dashed line).

Hence, the influence of buffer viscosity on FP<sub>16</sub> diffusion was studied by collecting single-molecule trajectories at different sucrose concentrations. Figure 5 shows relative values of the slow and fast diffusion coefficients as a function of solution viscosity. The fast diffusion component is seen to obey the SD equation semiquantitatively: at a buffer viscosity of  $9.7 \text{ cP}$ , it decreases by  $(21 \pm 5)\%$  compared to pure water. This small influence of the buffer viscosity is an indication that the fusion peptide is nicely inserted into the membrane. Surprisingly, the slow diffusion mode is affected much more strongly by the increased solution viscosity, with a change that is inversely dependent on the viscosity and decreases by  $(78 \pm 8)\%$  at  $9.7 \text{ cP}$ . This interesting result will be further discussed below. The rates of transition

between the slow and fast states were found to be independent of the solution viscosity. Only the insertion rate changed significantly, due to the decreased mobility of the peptides in solution.

**Effect of Temperature.** We tested the effect of temperature on the two diffusive modes by varying it between 10 and 40 °C. The temperature change affects both the membrane viscosity and the solution viscosity,<sup>61</sup> and the effect on the dynamics depends on which of the two has a more dominant role. We found that the relative fraction of molecules in the fast mode was temperature independent over the examined range of temperatures (Figure 6A).

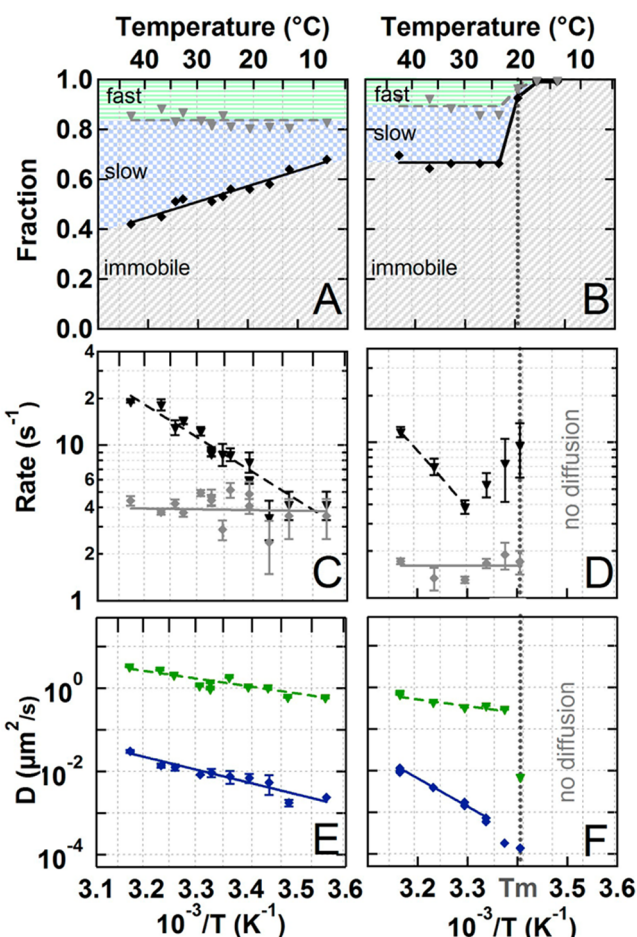


**Figure 6.** Effect of temperature on the dynamics of  $\text{FP}_{16}$  molecules in supported bilayers. Panels A, C, and E are for EPC membranes, whereas panels B, D, and F are for DMPC membranes. (A, B) Temperature dependence of the fractions of immobile molecules (gray) and molecules in the slow (blue) and fast (green) diffusive modes. (C, D) Arrhenius plots of the rates of transition between diffusive modes (fast to slow, black; slow to fast, gray). In this temperature range, EPC is in the liquid crystalline phase. (E, F) Arrhenius plots of the diffusion coefficients (fast diffusion, green; slow diffusion, blue) together with linear fits to the natural logarithms of the respective values. The fast diffusion coefficients were determined by JDA, the slow diffusion coefficients by MSD, as described in the text. The transition temperature of DMPC is 21 °C and is marked as a dotted line in parts B, D, and F.

The fraction of molecules in the slow mode effectively increased and the immobile fraction decreased as the temperature was increased, since the faster (absolute) diffusion allowed more and more slowly moving particles to pass our criterion and be counted as mobile. The rate of transition from the fast state to the

slow one showed a clear exponential dependence on inverse temperature, providing evidence for an activated process (Figure 6C). Using the Arrhenius equation, and assuming a temperature-independent frequency factor, we calculated an activation energy for this transition of  $(40.4 \pm 4.2)$  kJ/mol. The inverse transition (slow to fast) showed very weak dependence on temperature. All the other rates depicted in Figure 2A were temperature independent.

The diffusion coefficient of  $\text{FP}_{16}$  molecules was also measured as a function of temperature, and the results are plotted in Figure 6E. They depend exponentially on inverse temperature. Since the membrane viscosity is much higher than the solution viscosity (this is definitely correct for EPC, with  $\eta_m = 1.5 \text{ P}$  at 20 °C<sup>62</sup>), the diffusion is dominated by the temperature response of the former, which has a strong exponential dependence on temperature.<sup>56,62</sup> An alternative viewpoint can be obtained from the free volume model, which describes diffusion as a rate process,<sup>63,64</sup> and has also been used for analysis of diffusion within lipid membranes.<sup>65</sup> An Arrhenius-like behavior of the diffusion coefficient arises naturally within this model. We determined the apparent activation energy for the fast diffusion coefficient of  $\text{FP}_{16}$  in EPC membranes to be  $34 \pm 7$  kJ/mol, a value which is comparable to that of other membrane proteins.<sup>66,67</sup> Interestingly, a higher activation energy,  $56 \pm 6$  kJ/mol, was found for the slow diffusive mode. We compared these results to the diffusion of LissRhod-PE tracer molecules. The activation energy obtained with these molecules was  $38 \pm 8$  kJ/mol and hence in the range of the fast diffusion, as expected for non-interacting particles of similar size. This observation is also commensurate with literature findings (e.g., ref 68).

**What Happens Close to the Liquid Crystal to Gel Phase Transition?** To gain further understanding of the factors governing the formation of the slow and fast modes, we conducted experiments similar to the above using DMPC supported bilayers, whose liquid crystal to gel phase transition lies within the temperature range probed in our setup. The exact transition temperature of supported DMPC bilayers was experimentally determined by SPT measurements using a low density of LissRhod-PE lipid molecules. The phase transition was clearly observed as a drastic reduction of the diffusion coefficient of the lipids and was located at  $T_m = (21 \pm 1)$  °C (Supporting Information, Figure S11). This transition temperature is slightly lower than the known transition temperature of DMPC vesicles, 24 °C.<sup>69</sup>

In contrast to EPC membranes in which all mobile lipid molecules moved with the same diffusion coefficient, we observed that ~20% of the LissRhod-PE molecules diffused 10 times slower. The existence of a more slowly moving lipid fraction is common and often described in the literature (e.g., ref 28). However, it might complicate our analysis of slow and fast diffusive processes of  $\text{FP}_{16}$  molecules in DMPC membranes. We could verify, though, that for LissRhod-PE molecules no transitions between the two populations occurred, while  $\text{FP}_{16}$  molecules again showed clear transitions and diffusion coefficients in the ranges like those found for EPC, which allowed us to apply the three-state kinetic model to this system as well.

Well above the transition temperature, the rate of transition between fast and slow diffusive modes depended exponentially on temperature, with an activation energy of  $71.5 \pm 4.4$  kJ/mol, which is significantly larger than the activation energy measured in EPC membranes (Figure 6D). Unexpectedly, within the temperature region of the phase transition of DMPC, the rate of

transition from the fast to the slow mode was found to increase linearly. This implies that, as the membrane viscosity increases or as the phase transition nears, the transition into the slow diffusion is preferred. Just as in EPC, no dependence on temperature was found for the rate of transition from the slow mode back into the fast mode, either far from the phase transition or close to it (Figure 6D).

Figure 6F shows the Arrhenius plot of the diffusion coefficients of FP<sub>16</sub> molecules within the DMPC bilayer. The fast diffusion coefficient decreases by 2 orders of magnitude at the transition. Far above the transition temperature, the diffusion coefficient shows an Arrhenius-like dependence with an activation energy of  $31 \pm 7$  kJ/mol for the fast diffusive mode, which is comparable to EPC membranes, and  $130 \pm 9$  kJ/mol for the slow diffusive mode. It is interesting to note that as in EPC the activation energy of the slow diffusive mode is larger than that of the fast mode. The overall activation energy for LissRhod-PE in DMPC is also higher,  $95 \pm 11$  kJ/mol (Supporting Information, Figure S12). Below the transition temperature, nearly no diffusing particles, neither LissRhod-PE nor FP<sub>16</sub>, can be detected. The mobile fraction is less than 1% (Figure 6B).

**Effect of High Concentrations of Unlabeled FP.** Since it has been shown that FP<sub>16</sub> molecules may form  $\beta$ -sheet structured stacks within the membrane at relatively high concentrations,<sup>16</sup> we addressed the question of whether clustering might occur even when the solution concentration of the peptide is in the pM to nM range, and therefore might induce the observed slow diffusion. We added up to 100 nM of unlabeled FP<sub>16</sub> to 10 pM labeled FP<sub>16</sub> but could not find any concentration dependence, neither in the fraction of slow moving FP<sub>16</sub> nor in the diffusion coefficients of the two diffusive modes (see the Supporting Information, Figure S13). In addition, as the slow moving molecules had the same fluorescence intensity distribution as the fast moving ones, large clusters of labeled FP<sub>16</sub> molecules could be ruled out. In fact, even at the highest concentration used here (100 nM), the peptide/lipid ratio is  $\sim 1/7000$ , and is still in the range where monomers should be highly preferred and oligomerization of the peptides should play a very minor role.<sup>10</sup>

We also investigated the effect of high concentrations of FP<sub>16</sub> on the diffusion of lipid tracer molecules by adding increasing concentrations of unlabeled FP<sub>16</sub> while measuring lipid diffusion. For concentrations up to 10 nM (1000 times the concentration of a usual SPT experiment), we found no effect at all on the lipid diffusion. However, at 100 nM, a small lipid fraction of about 11% appeared to be moving approximately 30 times slower. Hence, the presence of FP<sub>16</sub> in the bilayer can influence the lipid diffusion, a finding which we will discuss in the following section.

#### What Might Be the Source of the Slow Diffusive Mode?

A significant finding of this work is the appearance of two diffusive modes in trajectories of FP<sub>16</sub>, slow and fast, and the possibility of interchange between them. The fast diffusive mode corresponds to the standard diffusion of peptides and proteins in supported bilayers. In this section, we attempt to find the source of the slow diffusive mode and speculate about its microscopic origin. One family of possible explanations for the appearance of the slow mode invokes structural imperfections or non-idealities related to the bilayer preparation process, especially when the vesicle fusion technique is used. For example, it was proposed in refs 33 and 70 that unruptured vesicles might remain weakly bound to the bilayer following its formation process, and could cause the appearance of an apparently slowly moving species. In order to check whether the appearance of two diffusive modes originates from the bilayer preparation method, or from other

local membrane defects as proposed in ref 31, we tracked highly diluted fluorescently labeled tracer molecules of LissRhod-PE embedded in the membrane. We found that 96% of all LissRhod-PE molecules are mobile, which agrees well with the results of similar experiments in the literature.<sup>38</sup> Furthermore, we did not observe any second slow diffusive mode and the MSD function was clearly linear with time (Figure S9A–C, Supporting Information). The extracted diffusion coefficient of  $2.1 \pm 0.1 \mu\text{m}^2/\text{s}$  agrees well with literature values obtained from fluorescence recovery after photobleaching (FRAP) measurements.<sup>71</sup> The MSD curve constructed from the temporal trajectories of the small fraction of LissRhod-PE molecules not classified as mobile was found to be completely flat, indicating that these are truly immobile molecules, rather than slowly moving ones. This experiment strongly suggests that weakly bound vesicles can be excluded as a source of the slow diffusion in our system.

Transient adsorption of tracer molecules onto the glass support, as proposed in ref 34, can most likely also be excluded as a cause of the slow diffusion, since that should lead to immobile, rather than slowly mobile, molecules. Further, for glass adsorption to occur, the FP<sub>16</sub> molecules should flip from the top leaflet of the membrane to the bottom leaflet, a process which is most likely too slow to be important on the time scale of interaction of peptides with the membrane.<sup>72,73</sup> Finally, at least in EPC membranes, the slow diffusion coefficient shows an Arrhenius behavior very similar to that of the fast diffusion coefficient, as well as that of the diffusion coefficient of LissRhod-PE, suggesting that it involves the membrane rather than the support. In the same manner, leaflet coupling with the glass support, as discussed in ref 32, does not explain our results. If a significant difference between the proximal and distal leaflets would exist, the experiments with LissRhod-PE should show two modes of diffusion with equal contribution. Moreover, as above, this process should be limited by peptide translocation across the bilayer, which is too slow. Finally, it was recently suggested that distortions of the whole membrane and formation of mobile pore-like structures might be responsible for the appearance of a slowly diffusing fraction.<sup>31</sup> This effect should have been observable in the LissRhod-PE experiments as well if it were of importance here. In conclusion, the slow diffusive mode seen in mobile particle trajectories is unlikely to be caused by membrane imperfections, and another explanation has to be sought out.

An important clue toward the interpretation of the slow diffusion is its dependence on solution viscosity, which deviates from the SD behavior,  $D \sim \ln(1/\eta_f)$ . Indeed, in Figure 5, we see that the slow diffusion coefficient follows a  $1/\eta_f$  dependence instead. One way to interpret this finding is that it arises from peptide molecules that are at the water–lipid interface and are not inserted into the membrane. Such molecules might be much more exposed to the buffer and hence possibly more sensitive to changes of the buffer viscosity. There is some evidence in the literature for adsorption of FP<sub>16</sub> molecules at the lipid–water interface under some conditions,<sup>13</sup> but it is not clear though why these helices should move much more slowly than inserted ones. In addition, we found that the activation energy of the slow diffusive mode, ( $59 \pm 6$ ) kJ/mol, is significantly higher than the activation energy of pure diffusion in water, 20.4 kJ/mol.<sup>74</sup> This suggests that the slow diffusive mode is not only influenced by the buffer viscosity but also by the membrane.

One is left with the possibility that the  $1/\eta_f$  dependence of the slow diffusive mode indicates the motion of objects which are large enough to obey eq 15. However, what can be the constituents of such large objects moving in the membrane?

One possibility might be the formation of aggregates or clusters of  $\text{FP}_{16}$  molecules. However, the low peptide/lipid ratio of  $1/10^6$  should lead to the presence of monomers only<sup>10</sup> and inspection of the distribution of fluorescence intensities of individual molecules, as well as measurements at high concentrations of unlabeled peptides (the peptide/lipid ratio is still not larger than  $1/7000$ ), allow us to conclude that the formation of (large) peptide clusters is negligible under our experimental conditions (Figure S13, Supporting Information). Thus, a likely explanation for the slow diffusive mode is the formation of some form of peptide–lipid complexes. Peptide–lipid interactions and locally induced membrane deformations are well-documented.<sup>53,75</sup> There are experimental indications that even small peptides can influence lipid diffusion,<sup>76–78</sup> and vice versa. Indeed, recent simulations support the idea that a protein can form a dynamic complex with surrounding lipid molecules, leading to concerted protein–lipid diffusion.<sup>79</sup>

On the basis of the diffusion coefficient of the slow mode and eq 15, we can estimate that the size of the peptide–lipid complex is  $\sim 350 \text{ nm}$ . This size is consistent with the requirement of eq 15,  $R > b$ . The exact number should not be taken too literally, though, as it depends on the approximations used in deriving this equation. Nevertheless, it is important to ask whether it is physically reasonable to assume that such large complexes exist in the membrane plane. One can answer in the affirmative in the case of DMPC, as the first-order liquid crystal to gel transition does not occur homogeneously across the membrane but rather leads to the formation of growing patches/domains as found by AFM measurements.<sup>80</sup> Therefore, there are at least two possible mechanisms for the formation of large peptide–lipid complexes in DMPC. First, it is possible that a peptide molecule induces a local perturbation which amounts to nucleation of a gel-like domain. Second, gel-like domains can form spontaneously, and diffusing peptide molecules may get trapped in these structures when crossing their border with the liquid crystalline areas of the membrane.

Indeed, we found that the rate of switching of  $\text{FP}_{16}$  molecules from the fast to the slow diffusive mode in DMPC membranes increased as the temperature was lowered below  $26^\circ\text{C}$  and down to the phase transition temperature. This observation supports the idea that the slow diffusive mode is caused by domains at different lipid order: the transition into the slow mode is more and more favored as the transition temperature is approached, and gel-like domains are more readily formed.

Most interestingly, the EPC membranes are studied much further away from the liquid crystal to gel transition temperature than the DMPC membranes, yet the slow diffusion is still observed. This might indicate that the phenomenon does not necessarily depend on the mobility of the lipids but on a property of the peptide. At high  $\text{FP}_{16}$  concentrations (peptide/lipid ratio of  $1/7000$ ), we observed an influence of the peptides on lipid diffusion while the diffusion of the peptides stayed unaffected. If we assume that those lipid molecules that are slowly moving in the presence of a high concentration of peptide molecules (11% of all molecules) are organized in clusters around single peptide molecules, a single cluster would consist of approximately 700 lipids. The area of such a large complex is  $\sim 490 \text{ nm}^2$  ( $A_{\text{lipid}} \approx 0.7 \text{ nm}^2$ <sup>81</sup>), which would result (according to eq 15) in an  $\sim 170$  times slower diffusion than that of a single  $\text{FP}_{16}$  helix with an approximate area of  $1.2 \times 2.5 \text{ nm}^2$  ( $R \sim 0.9 \text{ nm}$ ). Ignoring the many uncertainties involved in this calculation, this number would indeed be comparable to the experimental finding of a roughly 130 times slower diffusion.

An alternative type of peptide–lipid complex might form due to the effect of  $\text{FP}_{16}$  insertion into the outer leaflet on membrane properties, including induction of negative curvature<sup>5</sup> and reduction of the bending modulus.<sup>82</sup> It is possible that the outcome of these changes in membrane properties is a local protrusion of the membrane into the solution, which diffuses around together with the peptide (Figure 7B). Protrusions are

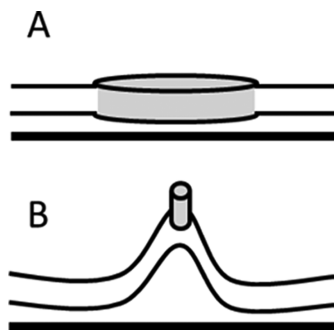


**Figure 7.** Schematic illustration of possible structural perturbations of a supported bilayer that may lead to slow diffusion. (A) A perturbation whose lateral dimension is significantly larger than the membrane height, such as a domain (either pre-existing or nucleated by the inserted peptide). (B) A local protrusion of the membrane, induced by the inserted peptide.

known to be formed by viral fusion peptides,<sup>83</sup> which are thought to facilitate reduction of the distance between the two membranes before fusion. The diffusion coefficient of such a protrusion may depend strongly on the solution viscosity,<sup>84,85</sup> as seen in the experiment. The formation of a protrusion can explain naturally the fact that an activation barrier exists for the transition from the fast diffusive mode to the slow one, if it requires detachment of the membrane from the substrate. On the other hand, the collapse of the protrusion and transition back to the fast diffusive mode is likely to be a barrier-less process. Further, the increase of the rate of transition from the fast to slow mode (Figure 6D) may be related in this picture to the reduction of the membrane bending modulus close to the transition temperature.<sup>86</sup> Using the value of the activation energy for the transition from the fast to the slow mode together with an estimate for the bilayer–substrate adhesion energy,<sup>87</sup> we calculate that  $\sim 7$  lipid molecules are involved in the formation of the protrusion. The obtained structure seems to be too small to explain the large reduction in the diffusion coefficient, but the calculated number of lipid molecules might easily be an underestimate.

## CONCLUSIONS

In this work, we used SPT to study the dynamics of a peptide derived from the HIV fusion protein,  $\text{FP}_{16}$ . This peptide was shown to readily incorporate into a supported lipid bilayer. Time-dependent diffusion trajectories of single  $\text{FP}_{16}$  molecules demonstrated switching between two diffusive modes. Subpopulations with different diffusion coefficients have long been observed in membrane studies, e.g., using FRAP. Our results suggest that such a behavior might not necessarily originate from two independent particle populations but can rather involve frequent and facile switching between modes, hidden in the analysis of bulk experiments. We used HMM analysis to identify and separate the diffusive modes, and also obtained the corresponding rates of transitions between them. The difference

in diffusion coefficients between the fast and slow modes was found to be as large as two orders of magnitude. Viscosity and temperature studies have led us to propose that the peptide molecules are involved in the formation of (temporary) lipid-peptide complexes of some form (such as domains), which diffuse in tandem. We discussed the possibility of induced local order (phases) of the lipids.

In future experiments, we will seek further evidence to support the existence of such structures even in EPC supported bilayers. In addition, we plan to look for a possible functional importance of the two modes of diffusion by studying the interaction of diffusing FP<sub>16</sub> molecules with peptides derived from the T-cell receptor. The current work is therefore expected to carry importance not only as new methodology for the analysis of complex membrane dynamics but also as an opening point for future studies of HIV pathogenesis.

## ■ ASSOCIATED CONTENT

### S Supporting Information

A detailed description of the microscopic setup (S1), the results of control experiments for choosing the most appropriate laser power (S2) and acquisition frequency (S3), the algorithms used to track diffusing particles (S4), the detailed descriptions of the analysis methods (S5), analysis of experimentally derived trajectories of (fixed) fluorescent spheres to determine the influence of the photon noise (S6), the algorithms used to simulate trajectories of particles allowed to switch between two diffusive states (S7), analysis results from simulated trajectories of unimodal diffusion (S8) as well as LissRhod-PE in EPC (S9) and DMPC (S11,S12), additional analysis details of the FP<sub>16</sub> diffusion in the absence (S10) and in the presence of unlabeled FP<sub>16</sub> (S13). This material is available free of charge via the Internet at <http://pubs.acs.org>.

## ■ AUTHOR INFORMATION

### Corresponding Author

\*Phone: 972-8-9342625 (G. H.). E-mail: gilad.haran@weizmann.ac.il (G. H.), maria.ott@physik.uni-halle.de (M. O.).

### Present Address

<sup>§</sup>Institute of Physics, Martin-Luther University Halle-Wittenberg, Von-Danckelmann-Platz 3, D-06120 Halle, Germany.

### Notes

The authors declare no competing financial interest.

## ■ ACKNOWLEDGMENTS

We would like to thank Profs. Haim Diamant (Tel Aviv University) and Nir Gov (Weizmann Institute) for educating us about membrane physics. We also thank Menahem Pirchi for his help with the implementation of the HMM analysis. The project was supported by a Minerva postdoctoral fellowship to M.O. and partially by the Israel Science Foundation. G.H. is the incumbent of the Hilda Pomeraniec Memorial Professorial Chair, and Y.S. is the incumbent of the Harold S. and Harriet B. Brady Professorial Chair in Cancer Research.

## ■ REFERENCES

- Alkhatib, G.; Combadiere, C.; Broder, C. C.; Feng, Y.; Kennedy, P. E.; Murphy, P. M.; Berger, E. A. CC CKRS: a RANTES, MIP-1alpha, MIP-1beta Receptor as a Fusion Cofactor for Macrophage-Tropic HIV-1. *Science* **1996**, *272*, 1955–1958.
- Kowalski, M.; Potz, J.; Basiripour, L.; Dorfman, T.; Goh, W. C.; Terwilliger, E.; Dayton, A.; Rosen, C.; Haseltine, W.; Sodroski, J. Functional Regions of the Envelope Glycoprotein of Human Immunodeficiency Virus Type 1. *Science* **1987**, *237*, 1351–1355.
- Wyatt, R.; Kwong, P. D.; Desjardins, E.; Sweet, R. W.; Robinson, J.; Hendrickson, W. A.; Sodroski, J. G. The Antigenic Structure of the HIV gp120 Envelope Glycoprotein. *Nature* **1998**, *393*, 705–711.
- Suarez, T.; Gallaher, W. R.; Aguirre, A.; Goni, F. M.; Nieva, J. L. Membrane Interface-Interacting Sequences within the Ectodomain of the Human Immunodeficiency Virus Type 1 Envelope Glycoprotein: Putative Role during Viral Fusion. *J. Virol.* **2000**, *74*, 8038–8047.
- Peisajovich, S. G.; Blank, L.; Epand, R. F.; Epand, R. M.; Shai, Y. On the Interaction between gp41 and Membranes: The Immunodominant Loop Stabilizes gp41 Helical Hairpin Conformation. *J. Mol. Biol.* **2003**, *326*, 1489–1501.
- Chan, D. C.; Kim, P. S. HIV Entry and Its Inhibition. *Cell* **1998**, *93*, 681–684.
- Weissenhorn, W.; Dessen, A.; Calder, L. J.; Harrison, S. C.; Skehel, J. J.; C., W. D. Structural Basis for Membrane Fusion by Enveloped Viruses. *Mol. Membr. Biol.* **1999**, *16*, 3–9.
- Gordon, L. M.; Mobley, P. W.; Lee, W.; Eskandari, S.; Kaznessis, Y. N.; Sherman, M. A.; Waring, A. J. Conformational Mapping of the N-Terminal Peptide of HIV-1 gp41 in Lipid Detergent and Aqueous Environments Using <sup>13</sup>C-Enhanced Fourier Transform Infrared Spectroscopy. *Protein Sci.* **2004**, *13*, 1012–1030.
- Gordon, L. M.; Mobley, P. W.; Pilpa, R.; Sherman, M. A.; Waring, A. J. Conformational Mapping of the N-Terminal Peptide of HIV-1 gp41 in Membrane Environments Using <sup>13</sup>C-Enhanced Fourier Transform Infrared Spectroscopy. *Biochim. Biophys. Acta, Biomembr.* **2002**, *1559*, 96–120.
- Curtain, C.; Separovic, F.; Nielsen, K.; Craik, D.; Zhong, Y.; Kirkpatrick, A. The Interactions of the N-Terminal Fusogenic Peptide of HIV-1 gp41 with Neutral Phospholipids. *Eur. Biophys. J.* **1999**, *28*, 427–436.
- Jaroniec, C. P.; Kaufman, J. D.; Stahl, S. J.; Viard, M.; Blumenthal, R.; Wingfield, P. T.; Bax, A. Structure and Dynamics of Micelle-Associated Human Immunodeficiency Virus gp41 Fusion Domain. *Biochemistry* **2005**, *44*, 16167–16180.
- Li, Y.; Tamm, L. K. Structure and Plasticity of the Human Immunodeficiency Virus gp41 Fusion Domain in Lipid Micelles and Bilayers. *Biophys. J.* **2007**, *93*, 876–885.
- Martin, I.; Defrise-Quertain, F.; Decroly, E.; Vandendanden, M.; Brasseur, R.; Ruysschaert, J.-M. Orientation and Structure of the NH<sub>2</sub>-Terminal HIV-1 gp41 Peptide in Fused and Aggregated Liposomes. *Biochim. Biophys. Acta, Biomembr.* **1993**, *1145*, 124–133.
- Yang, J.; Prorok, M.; Castellino, F. J.; Weliky, D. P. Oligomeric  $\beta$ -Structure of the Membrane-Bound HIV-1 Fusion Peptide Formed from Soluble Monomers. *Biophys. J.* **2004**, *87*, 1951–1963.
- Sackett, K.; Shai, Y. The HIV Fusion Peptide Adopts Intermolecular Parallel  $\beta$ -Sheet Structure in Membranes When Stabilized by the Adjacent N-Terminal Heptad Repeat: A <sup>13</sup>C FTIR Study. *J. Mol. Biol.* **2005**, *350*, 790–805.
- Cohen, T.; Pevsner-Fischer, M.; Cohen, N.; Cohen, I. R.; Shai, Y. Characterization of the Interacting Domain of the HIV-1 Fusion Peptide with the Transmembrane Domain of the T-Cell Receptor. *Biochemistry* **2008**, *47*, 4826–4833.
- Mobley, P. W.; Waring, A. J.; Sherman, M. A.; Gordon, L. M. Membrane Interactions of the Synthetic N-Terminal Peptide of HIV-1 gp41 and Its Structural Analogs. *Biochim. Biophys. Acta, Biomembr.* **1999**, *1418*, 1–18.
- Nieva, J. L.; Nir, S.; Muga, A.; Goni, F. M.; Wilschut, J. Interaction of the HIV-1 Fusion Peptide with Phospholipid Vesicles: Different Structural Requirements for Fusion and Leakage. *Biochemistry* **1994**, *33*, 3201–3209.
- Rafalski, M.; Lear, J. D.; DeGrado, W. F. Phospholipid Interactions of Synthetic Peptides Representing the N-Terminus of HIV gp41. *Biochemistry* **1990**, *29*, 7917–7922.
- MacDonald, R. I. Characteristics of Self-Quenching of the Fluorescence of Lipid-Conjugated Rhodamine in Membranes. *J. Biol. Chem.* **1990**, *265*, 13533–13539.

- (21) Maddox, M. W.; Longo, M. L. Conformational Partitioning of the Fusion Peptide of HIV-1 gp41 and Its Structural Analogs in Bilayer Membranes. *Biophys. J.* **2002**, *83*, 3088–3096.
- (22) Gabrys, C. M.; Qiang, W.; Sun, Y.; Xie, L.; Schmick, S. D.; Weliky, D. P. Solid-State Nuclear Magnetic Resonance Measurements of HIV Fusion Peptide  $^{13}\text{CO}$  to Lipid 31P Proximities Support Similar Partially Inserted Membrane Locations of the  $\alpha$ -Helical and  $\beta$ -Sheet Peptide Structures. *J. Phys. Chem. A* **2013**, DOI: 10.1021/jp312845w.
- (23) Tanaka, M.; Sackmann, E. Polymer-Supported Membranes as Models of the Cell Surface. *Nature* **2005**, *437*, 656–663.
- (24) Elson, E. L.; Magde, D. Fluorescence Correlation Spectroscopy. I. Conceptual Basis and Theory. *Biopolymers* **1974**, *13*, 1–27.
- (25) Axelrod, D.; Koppel, D.; Schlessinger, J.; Elson, E.; Webb, W. Mobility Measurement by Analysis of Fluorescence Photobleaching Recovery Kinetics. *Biophys. J.* **1976**, *16*, 1055–1069.
- (26) Saxton, M. Lateral Diffusion in an Archipelago. Single-Particle Diffusion. *Biophys. J.* **1993**, *64*, 1766–1780.
- (27) Grünwald, D.; Martin, R. M.; Buschmann, V.; Bazett-Jones, D. P.; Leonhardt, H.; Kubitscheck, U.; Cardoso, M. C. Probing Intracellular Environments at the Single-Molecule Level. *Biophys. J.* **2008**, *94*, 2847–2858.
- (28) Schütz, G.; Schindler, H.; Schmidt, T. Single-Molecule Microscopy on Model Membranes Reveals Anomalous Diffusion. *Biophys. J.* **1997**, *73*, 1073–1080.
- (29) Thompson, R. E.; Larson, D. R.; Webb, W. W. Precise Nanometer Localization Analysis for Individual Fluorescent Probes. *Biophys. J.* **2002**, *82*, 2775–2783.
- (30) Widengren, J.; Rigler, R. Mechanisms of Photobleaching Investigated by Fluorescence Correlation Spectroscopy. *Bioimaging* **1996**, *4*, 149–157.
- (31) Sharonov, A.; Bandichhor, R.; Burgess, K.; Petrescu, A. D.; Schroeder, F.; Kier, A. B.; Hochstrasser, R. M. Lipid Diffusion from Single Molecules of a Labeled Protein Undergoing Dynamic Association with Giant Unilamellar Vesicles and Supported Bilayers. *Langmuir* **2008**, *24*, 844–850.
- (32) Scomparin, C.; Lecuyer, S.; Ferreira, M.; Charitat, T.; Tinland, B. Diffusion in Supported Lipid Bilayers: Influence of Substrate and Preparation Technique on the Internal Dynamics. *Eur. Phys. J. E* **2009**, *28*, 211–220.
- (33) Chiantia, S.; Kahya, N.; Schwille, P. Raft Domain Reorganization Driven by Short- and Long-Chain Ceramide: A Combined AFM and FCS Study. *Langmuir* **2007**, *23*, 7659–7665.
- (34) Dertinger, T.; von der Hocht, I.; Benda, A.; Hof, M.; Enderlein, J. Surface Sticking and Lateral Diffusion of Lipids in Supported Bilayers. *Langmuir* **2006**, *22*, 9339–9344.
- (35) Kubitscheck, U.; Wedekind, P.; Peters, R. Lateral Diffusion Measurement at High Spatial Resolution by Scanning Microphotolysis in a Confocal Microscope. *Biophys. J.* **1994**, *67*, 948–956.
- (36) Burns, A.; Frankel, D.; Buranda, T. Local Mobility in Lipid Domains of Supported Bilayers Characterized by Atomic Force Microscopy and Fluorescence Correlation Spectroscopy. *Biophys. J.* **2005**, *89*, 1081–1093.
- (37) Wang, T.; Ingram, C.; Weisshaar, J. C. Model Lipid Bilayer with Facile Diffusion of Lipids and Integral Membrane Proteins. *Langmuir* **2010**, *26*, 11157–11164.
- (38) Murray, D. H.; Tamm, L. K.; Kiessling, V. Supported Double Membranes. *J. Struct. Biol.* **2009**, *168*, 183–189.
- (39) Sonnleitner, A.; Schütz, G.; Schmidt, T. Free Brownian Motion of Individual Lipid Molecules in Biomembranes. *Biophys. J.* **1999**, *77*, 2638–2642.
- (40) Rabiner, L. A Tutorial on Hidden Markov Models and Selected Applications in Speech Recognition. *Proc. IEEE* **1989**, *77*, 257–286.
- (41) Montiel, D.; Cang, H.; Yang, H. Quantitative Characterization of Changes in Dynamical Behavior for Single-Particle Tracking Studies. *J. Phys. Chem. B* **2006**, *110*, 19763–19770.
- (42) Elliott, L. C. C.; Barhoum, M.; Harris, J. M.; Bohn, P. W. Trajectory Analysis of Single Molecules Exhibiting Non-Brownian Motion. *Phys. Chem. Chem. Phys.* **2011**, *13*, 4326–4334.
- (43) Das, R.; Cairo, C. W.; Coombs, D. A Hidden Markov Model for Single Particle Tracks Quantifies Dynamic Interactions between LFA-1 and the Actin Cytoskeleton. *PLoS Comput. Biol.* **2009**, *5*, e1000556.
- (44) Persson, F.; Linden, M.; Unoson, C.; Elf, J. Extracting Intracellular Diffusive States and Transition Rates From Single-Molecule Tracking Data. *Nat. Methods* **2013**, *10*, 265–269.
- (45) Bloch, I.; Quintana, F. J.; Gerber, D.; Cohen, T.; Cohen, I. R.; Shai, Y. T-Cell Inactivation and Immunosuppressive Activity Induced by HIV gp41 via Novel Interacting Motif. *FASEB J.* **2007**, *21*, 393–401.
- (46) Boukobza, E.; Sonnenfeld, A.; Haran, G. Immobilization in Surface-Tethered Lipid Vesicles as a New Tool for Single Biomolecule Spectroscopy. *J. Phys. Chem. B* **2001**, *105*, 12165–12170.
- (47) Ruprecht, V.; Bramshuber, M.; Schutz, G. J. Two-Color Single Molecule Tracking Combined with Photobleaching for the Detection of Rare Molecular Interactions in Fluid Biomembranes. *Soft Matter* **2010**, *6*, 568–581.
- (48) Widengren, J.; Chmyrov, A.; Eggeling, C.; Löfdahl, P.-A.; Seidel, C. A. M. Strategies to Improve Photostabilities in Ultrasensitive Fluorescence Spectroscopy. *J. Phys. Chem. A* **2007**, *111*, 429–440.
- (49) Serge, A.; Bertaux, N.; Rigneault, H.; Marguet, D. Dynamic Multiple-Target Tracing to Probe Spatiotemporal Cartography of Cell Membranes. *Nat. Methods* **2008**, *5*, 687–694.
- (50) Jaqaman, K.; Loerke, D.; Mettlen, M.; Kuwata, H.; Grinstein, S.; Schmid, S. L.; Danuser, G. Robust Single-Particle Tracking in Live-Cell Time-Lapse Sequences. *Nat. Methods* **2008**, *5*, 695–702.
- (51) Saxton, M. Single-Particle Tracking: the Distribution of Diffusion Coefficients. *Biophys. J.* **1997**, *72*, 1744–1753.
- (52) Murphy, K. Hidden Markov Model (HMM) Toolbox for Matlab, 1998, <http://www.cs.ubc.ca/murphyk/Software/HMM/hmm.html>.
- (53) Gambin, Y.; Lopez-Esparza, R.; Reffay, M.; Sierecki, E.; Gov, N. S.; Genest, M.; Hodges, R. S.; Urbach, W. Lateral Mobility of Proteins in Liquid Membranes Revisited. *Proc. Natl. Acad. Sci. U.S.A.* **2006**, *103*, 2098–2102.
- (54) Ramadurai, S.; Holt, A.; Krasnikov, V.; van den Bogaart, G.; Killian, J. A.; Poolman, B. Lateral Diffusion of Membrane Proteins. *J. Am. Chem. Soc.* **2009**, *131*, 12650–12656.
- (55) Saffman, P. G. Brownian Motion in Thin Sheets of Viscous Fluid. *J. Fluid Mech.* **1976**, *73*, 593.
- (56) Cicuta, P.; Keller, S. L.; Veatch, S. L. Diffusion of Liquid Domains in Lipid Bilayer Membranes. *J. Phys. Chem. B* **2007**, *111*, 3328–3331.
- (57) Evans, E.; Sackmann, E. Translational and Rotational Drag Coefficients for a Disk Moving in a Liquid Membrane Associated with a Rigid Substrate. *J. Fluid Mech.* **1988**, *194*, 553–561.
- (58) Stone, H.; Armand Ajdar, I. Hydrodynamics of Particles Embedded in a Flat Surfactant Layer Overlying a Subphase of Finite Depth. *J. Fluid Mech.* **1998**, *369*, 151–173.
- (59) Peters, R.; Cherry, R. J. Lateral and Rotational Diffusion of Bacteriorhodopsin in Lipid Bilayers - Experimental Test of the Saffman-Delbrück Equations. *Proc. Natl. Acad. Sci. U.S.A.* **1982**, *79*, 4317–4321.
- (60) Vaz, W. L. C.; Clegg, R. M.; Hallmann, D. Translational Diffusion of Lipids in Liquid Crystalline Phase Phosphatidylcholine Multibilayers. A Comparison of Experiment with Theory. *Biochemistry* **1985**, *24*, 781–786.
- (61) Korson, L.; Drost-Hansen, W.; Millero, F. J. Viscosity of Water at Various Temperatures. *J. Phys. Chem.* **1969**, *73*, 34–39.
- (62) Cogan, U.; Shinitzky, M.; Weber, G.; Nishida, T. Microviscosity and Order in the Hydrocarbon Region of Phospholipid and Phospholipid-Cholesterol Dispersions Determined with Fluorescent Probes. *Biochemistry* **1973**, *12*, 521–528.
- (63) Glasstone, S.; Laidler, K. J.; Eyring, H. *The Theory of Rate Processes: the Kinetics of Chemical Reactions, Viscosity, Diffusion and Electrochemical Phenomena*; McGraw-Hill Book Co.: New York, London, 1941; Chapter IX.
- (64) Cohen, M. H.; Turnbull, D. Molecular Transport in Liquids and Glasses. *J. Chem. Phys.* **1959**, *31*, 1164.
- (65) Galla, H. J.; Hartmann, W.; Theilen, U.; Sackmann, E. On Two-Dimensional Passive Random Walk in Lipid Bilayers and Fluid Pathways in Biomembranes. *J. Membr. Biol.* **1979**, *48*, 215–236.

- (66) Gaede, H. C.; Gawrisch, K. Lateral Diffusion Rates of Lipid, Water, and a Hydrophobic Drug in a Multilamellar Liposome. *Biophys. J.* **2003**, *85*, 1734–1740.
- (67) Vaz, W. L. C.; Criado, M.; Madeira, V. M. C.; Schoellmann, G.; Jovin, T. M. Size Dependence of the Translational Diffusion of Large Integral Membrane Proteins in Liquid-Crystalline Phase Lipid Bilayers. A Study Using Fluorescence Recovery after Photobleaching. *Biochemistry* **1982**, *21*, 5608–5612.
- (68) Vaz, W. L.; Dieter, H. Experimental Evidence against the Applicability of the Saffman-Delbrück Model to the Translational Diffusion of Lipids in Phosphatidylcholine Bilayer Membranes. *FEBS Lett.* **1983**, *152*, 287–290.
- (69) Needham, D.; Evans, E. Structure and Mechanical Properties of Giant Lipid (DMPC) Vesicle Bilayers from 20 °C below to 10 °C above the Liquid Crystal-Crystalline Phase Transition at 24.degree.C. *Biochemistry* **1988**, *27*, 8261–8269.
- (70) Machán, R.; Hof, M. Lipid Diffusion in Planar Membranes Investigated by Fluorescence Correlation Spectroscopy. *Biochim. Biophys. Acta, Biomembr.* **2010**, *1798*, 1377–1391.
- (71) Seu, K. J.; Cambrea, L. R.; Everly, R. M.; Hovis, J. S. Influence of Lipid Chemistry on Membrane Fluidity: Tail and Headgroup Interactions. *Biophys. J.* **2006**, *91*, 3727–3735.
- (72) Takeshima, K.; Chikushi, A.; Lee, K.-K.; Yonehara, S.; Matsuzaki, K. Translocation of Analogs of the Antimicrobial Peptides Magainin and Buforin across Human Cell Membranes. *J. Biol. Chem.* **2003**, *278*, 1310–1315.
- (73) Stella, L.; Burattini, M.; Mazzuca, C.; Palleschi, A.; Venanzi, M.; Coin, I.; Peggion, C.; Toniolo, C.; Pispisa, B. Alamethicin Interaction with Lipid Membranes: A Spectroscopic Study on Synthetic Analogs. *Chem. Biodiversity* **2007**, *4*, 1299–1312.
- (74) Wassall, S. Pulsed Field Gradient-Spin Echo NMR Studies of Water Diffusion in a Phospholipid Model Membrane. *Biophys. J.* **1996**, *71*, 2724–2732.
- (75) Tampe, R.; Von Lukas, A.; Galla, H. J. Glycophorin-Induced Cholesterol-Phospholipid Domains in Dimyristoylphosphatidylcholine Bilayer Vesicles. *Biochemistry* **1991**, *30*, 4909–4916.
- (76) Sheynis, T.; Sykora, J.; Benda, A.; Kolusheva, S.; Hof, M.; Jelinek, R. Bilayer Localization of Membrane-Active Peptides Studied in Biomimetic Vesicles by Visible and Fluorescence Spectroscopies. *Eur. J. Biochem.* **2003**, *270*, 4478–4487.
- (77) Guo, L.; Smith-Dupont, K. B.; Gai, F. Diffusion as a Probe of Peptide-Induced Membrane Domain Formation. *Biochemistry* **2011**, *50*, 2291–2297.
- (78) Smith-Dupont, K. B.; Guo, L.; Gai, F. Diffusion as a Probe of the Heterogeneity of Antimicrobial Peptide-Membrane Interactions. *Biochemistry* **2010**, *49*, 4672–4678.
- (79) Niemela, P. S.; Miettinen, M. S.; Monticelli, L.; Hammaren, H.; Bjelkmar, P.; Murtola, T.; Lindahl, E.; Vattulainen, I. Membrane Proteins Diffuse as Dynamic Complexes with Lipids. *J. Am. Chem. Soc.* **2010**, *132*, 7574–7575.
- (80) Tokumasu, F.; Jin, A. J.; Feigenson, G. W.; Dvorak, J. A. Atomic Force Microscopy of Nanometric Liposome Adsorption and Nanoscopic Membrane Domain Formation. *Ultramicroscopy* **2003**, *97*, 217–227.
- (81) Petracche, H. I.; Tristram-Nagle, S.; Nagle, J. F. Fluid Phase Structure of EPC and DMPC Bilayers. *Chem. Phys. Lipids* **1998**, *95*, 83–94.
- (82) Shchelokovskyy, P.; Tristram-Nagle, S.; Dimova, R. Effect of the HIV-1 Fusion Peptide on the Mechanical Properties and Leaflet Coupling of Lipid Bilayers. *New J. Phys.* **2011**, *13*, 025004.
- (83) Martens, S.; McMahon, H. T. Mechanisms of Membrane Fusion: Disparate Players and Common Principles. *Nat. Rev. Mol. Cell Biol.* **2008**, *9*, 543–556.
- (84) Naji, A.; Levine, A. J.; Pincus, P. Corrections to the Saffman-Delbrück Mobility for Membrane Bound Proteins. *Biophys. J.* **2007**, *93*, L49–L51.
- (85) Naji, A.; Atzberger, P. J.; Brown, F. L. H. Hybrid Elastic and Discrete-Particle Approach to Biomembrane Dynamics with Application to the Mobility of Curved Integral Membrane Proteins. *Phys. Rev. Lett.* **2009**, *102*, 138102.
- (86) Lecuyer, S.; Charitat, T. From Supported Membranes to Tethered Vesicles: Lipid Bilayers Destabilisation at the Main Transition. *Europhys. Lett.* **2006**, *75*, 652.
- (87) Goldberg, R.; Schroeder, A.; Silbert, G.; Turjeman, K.; Barenholz, Y.; Klein, J. Boundary Lubricants with Exceptionally Low Friction Coefficients Based on 2D Close-Packed Phosphatidylcholine Liposomes. *Adv. Mater.* **2011**, *23*, 3517–3521.